Hindawi
International Journal of Antennas and Propagation
Volume 2017, Article ID 5619728, 13 pages
https://doi.org/10.1155/2017/5619728

Review Article

A Review of Sensing Strategies for Microwave Sensors Based on Metamaterial-Inspired Resonators: Dielectric Characterization, Displacement, and Angular Velocity Measurements for Health Diagnosis, Telecommunication, and Space Applications

Lijuan Su, Javier Mata-Contreras, Paris Vélez, and Ferran Martín

CIMITEC, Departament d'Enginyeria Electrònica, Universitat Autònoma de Barcelona, 08193 Bellaterra, Spain

Correspondence should be addressed to Lijuan Su; lijuan.su@uab.cat

Received 17 January 2017; Accepted 9 March 2017; Published 14 May 2017

Academic Editor: Mirko Barbuto

Four sensing approaches for the implementation of microwave sensors based on transmission lines loaded with metamaterial-inspired resonators are considered in this review paper, and examples of applications are pointed out. In all the cases, sensing is based on the effects that the magnitude under measurement causes in the transmission properties of the resonator-loaded line. Such four strategies are (i) resonance frequency variation, (ii) coupling modulation through symmetry disruption (causing variation of the notch depth), (iii) frequency splitting (also exploiting symmetry properties), and (iv) amplitude modulation of a harmonic signal. Such sensors are useful in various scenarios, of interest in fields as diverse as characterization of dielectric materials for communication circuits, medical diagnosis and treatment with microwave technologies, and sensors for space applications, among others.

1. Introduction

Metamaterial-inspired resonators are electrically small resonant particles useful for the implementation of one-dimensional (e.g., metamaterial transmission lines [1]), two-dimensional (e.g., metasurfaces [2]), and three-dimensional (e.g., lenses for MRI [3]) metamaterials. Such resonant elements are "atoms" (sometimes called "meta-atoms"), which can be structured (or engineered) to form periodic artificial materials with unusual electromagnetic properties (negative refraction [4], backward wave propagation [5] and radiation [6], slow and fast waves [4–7], cloaking [8], etc.). Such properties, in general, arise as long as the composite acts as an effective medium for the electromagnetic field with which it interacts. In an effective medium, the properties can be tailored to some extent and are different from those of the constitutive elements, typically conventional metals and dielectrics in most metamaterials (obviously, this does not exclude the use of advanced materials, such as ferroelectrics [9, 10], liquid crystals [11, 12], and graphene [13], or components, such as microelectromechanical systems—MEMS [14, 15]). A well-known example of unusual (effective medium) property is the negative refractive index achievable in composites made of split ring resonators (SRRs) and metallic strips (or posts), related to the simultaneous negative effective permeability (due to the SRRs) and permittivity (related to the metallic strips) of the structure [7]. Key to achieve such effective medium properties is the characteristic dimension (period) of the composite, which must be much smaller than the wavelength of the illuminating radiation. In this regard, metamaterial-inspired resonators are semilumped elements with electrical size significantly smaller than the wavelength at their fundamental resonance frequency, and hence they are useful particles ("atoms") for the implementation of metamaterials. Examples of such resonant elements are the SRR [16], the complementary split ring resonator (CSRR) [17], the broadside coupled SRR (BC-SRR) [18], the electric LC (ELC) resonator [19], the S-shaped SRR (S-SRR) [20],

the folded SIR (F-SIR) [21], and many others (the authors recommend the book [22] for an exhaustive list, analysis, and applications of such resonant particles).

Besides these effective medium properties, which arise in periodic (or quasi-periodic) structures made of the previous (or other) metamaterial resonators and are useful for the implementation of microwave components with small size or superior performance or based on novel functionalities [1, 22], it is possible to use the resonance, electrical size, shape, and specific properties of some metamaterial resonators in other applications, including sensing (the purpose of this review article). Metamaterial-inspired resonators are very useful particles for the implementation of compact, high-sensitivity, and robust sensors on the basis of different strategies or approaches, for applications as diverse as characterization of dielectric materials for communication circuits, medical diagnosis and treatment with microwave technologies, and sensors for space applications, among others.

In this paper, four sensing approaches for the implementation of microwave sensors based on metamaterial resonators are reviewed, and examples of applications are pointed out. In all the cases, the sensing strategies are based on transmission lines loaded with such resonant elements. Such lines resemble metamaterial transmission lines, but the resonance phenomenon, rather than effective medium properties, is exploited. Such sensing strategies are resonance frequency variation, coupling modulation through symmetry disruption (causing variation of the notch depth), frequency splitting (also exploiting symmetry properties), and amplitude modulation of a harmonic signal.

2. Sensing Strategies

In this section, the four sensing strategies (or principles) are reviewed, whereas some applications of them are included in the next section.

2.1. Sensors Based on Frequency Variation. A transmission line loaded with a resonant element (either coupled to it or in contact with it) exhibits a set of transmission zeros (notches) in the frequency response. These transmission zeros occur at those frequencies where the resonant element produces an open or a virtual ground to the line, and the injected power is completely reflected back at these frequencies (excluding the effects of losses). Typically, the frequency of interest for microwave circuit and sensor design is the first (fundamental) resonance frequency, where metamaterial resonators can be used in order to achieve compact dimensions. This frequency (and higher order harmonic frequencies) may be altered by the effects of external stimulus or perturbations (e.g., moisture, temperature), by the relative position or orientation between the line and the resonant element (distance, lateral displacement, etc.), or by the presence of substances/materials surrounding the resonant element. Therefore, it follows that resonance frequency variation can be used for sensing many different variables, including position, velocity, material characteristics (e.g., permittivity), and moisture. These sensors are in general very simple but may suffer from cross-sensitivities, defined as the sensitivity of the sensors to other variables different from the one of interest (measurand). For example, since permittivity depends on environmental conditions (e.g., temperature), the resonance frequency can be unintentionally shifted by spurious effects in permittivity sensors. Nevertheless, in many applications, external factors such as temperature or humidity do not experience significant variations. Moreover, these frequency variation based sensors are typically calibrated for accurate measurements. Therefore, these sensors are useful in many applications where design simplicity and low cost are key aspects.

2.2. Coupling Modulation Based Sensors. This sensing approach belongs to the so-called symmetry-based sensing [22–24], where symmetry properties are exploited for the implementation of sensors. In these sensors, a transmission line is loaded with a single symmetric resonator (electromagnetically coupled to the line), and the sensing principle is the control of the level of coupling between the line and the resonator, caused by the measurand and related to disruption of symmetry. These sensors are particularly useful for the measurement of spatial variables (e.g., alignment, displacement, and velocity) [24–27], and in this case the resonator is etched on a substrate (or object) different from that of the transmission line, in order to allow for a relative motion between the line and the resonator. However, symmetry can also be disrupted by asymmetric dielectric loading of the resonant element.

In these sensors, the symmetry plane of the transmission line is aligned with the symmetry plane of the resonant element, and both symmetry planes must be of different electromagnetic nature (one an electric wall and the other one a magnetic wall). Under these conditions, line-to-resonator coupling is prevented, and the structure exhibits total transmission. Conversely, by breaking symmetry through the effects of the variable under measurement (e.g., a spatial variable), a transmission zero, or notch, appears, and the notch depth depends on the level of asymmetry, since such level determines the magnitude of electromagnetic coupling between the line and the resonant element. Figure 1 illustrates this sensing principle, where symmetry disruption is caused by lateral displacement of the resonant element, a SRR, and the considered transmission line is a CPW. It is interesting to mention that, for the parasitic slot mode (odd mode) of the CPW transmission line, where the axial plane is an electric wall, rather than a magnetic wall, the structure exhibits a notch when the SRR is symmetrically loaded.

As compared to the previous approach, a key advantage of coupling modulation sensors is their robustness against variable environmental conditions. The reason is that the principle of operation relies on geometrical alignment/misalignment, which cannot be altered by environmental factors. Although these sensors cannot be considered to be true differential sensors, indeed they exhibit a similar behavior since the net coupling between the line and the resonator can be expressed in terms of the difference between partial couplings related to each half of the structure [32]. The output variable in these sensors is the notch depth expressed in dB (as usual to quantify attenuation). A disadvantage of these

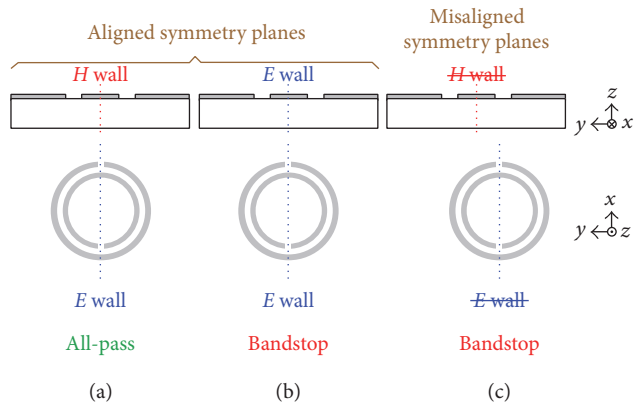

Figure 1: CPW transmission line loaded with a single SRR. (a) Line and resonator aligned and excitation with the fundamental (even) mode; (b) line and resonator aligned and excitation with the slot (odd) mode; (c) line and resonator misaligned and excitation with the fundamental (even) mode. It is apparent that, for misaligned loadings, the magnetic wall at the symmetry plane of the line is altered.

sensors is, therefore, their susceptibility to electromagnetic interference (EMI) and noise. Nevertheless, the resonance frequency of the resonant element can be tailored in order to avoid interfering signals (if they are present). Shielding of the sensors is also an alternative to mitigate the effects of EMI. For the measurement of spatial variables, these sensors are very interesting since the measurement can be contactless (by means of an air gap between the line and the resonator). By this means, mechanical friction is avoided, and aging effects are less severe as compared to sensors where friction is present, such as in rotary potentiometers [33].

2.3. Frequency Splitting Sensors. In this approach, the sensors are composed of a transmission line loaded with a pair of resonators in a symmetric configuration. The sensing principle is based on resonance frequency splitting. Thus, in the reference (symmetric) state, the structure exhibits a single notch, but two notches appear when symmetry is disrupted, and the frequency separation between them is related to the level of asymmetry [23].

Typically, these sensors find applications in material characterization. A test region in the vicinity of the resonators should be defined. By adding a material or substance in those regions, a single transmission zero appears if the material distribution (specifically the permittivity) is symmetric. On the contrary, if the material loading is not symmetric, two notches in the transmission coefficient, indicative of such asymmetry, arise. Note that this strategy is useful for the implementation of sensors and comparators. Such sensors are differential sensors, able to provide the difference between two permittivity values. As a comparator, the structure solely compares two permittivities, indicating whether their values are the same or not. This latter application is useful for the detection of defects or abnormalities in material samples as compared to a well-known reference. Similar to the previous sensing approach, frequency splitting sensors are robust in front of changing environmental conditions since a true differential measurement is performed in such sensors.

One important drawback of these frequency splitting sensors is the coupling between resonators, unavoidable if these resonators are close enough. Coupling tends to degrade sensor performance, specifically the sensitivity at small perturbations, as reported in [34]. To circumvent the coupling between resonant elements, one possibility is to cascade the resonant elements [35]. By this means, the structure is not necessarily symmetric, but the working principle is exactly the same. However, if the resonators are separated enough, coupling no longer arises. Alternatively, a divider/combiner configuration, where each transmission line branch is loaded with a resonant element, can be considered [30, 36]. In this case, coupling is prevented, but, in general, the two notches for the asymmetric configuration are related to an interference phenomenon. The result is that sensitivity is degraded as well, unless the lengths of the transmission line sections of the splitter/combiner are appropriately chosen [30, 36]. Figure 2 depicts the three considered configurations, where the resonant element is a stepped impedance resonator (SIR).

As reported in [30], the electrical lengths of the transmission line sections connecting the Y-junction of the divider/combiner with the plane where the SIRs are connected (Figure 2(c)) must be exactly π at the fundamental resonance frequency of the SIRs. With this choice, the shorts at the plane where the SIRs are connected to the lines are translated to the Y-junction, and a transmission zero at the frequency of the SIRs arises. By disrupting symmetry by altering one of the SIRs (e.g., by means of a dielectric load), the transmission zero at the SIRs frequency prevails, whereas the other one is a consequence of an interfering phenomenon. The fact that one of the transmission zeros is kept unaltered regardless of the level of asymmetry explains the optimized sensitivity under the mentioned conditions relative to the electrical length of the divider/combiner transmission line sections. Importantly, if the previous conditions are satisfied, the two notches that appear for the asymmetric case are quite similar. This is interesting in order to properly detect small perturbations (asymmetries).

2.4. Amplitude Modulation Based Sensors. These sensors consist of a transmission line fed by a harmonic signal tuned at the fundamental frequency of a certain resonator coupled

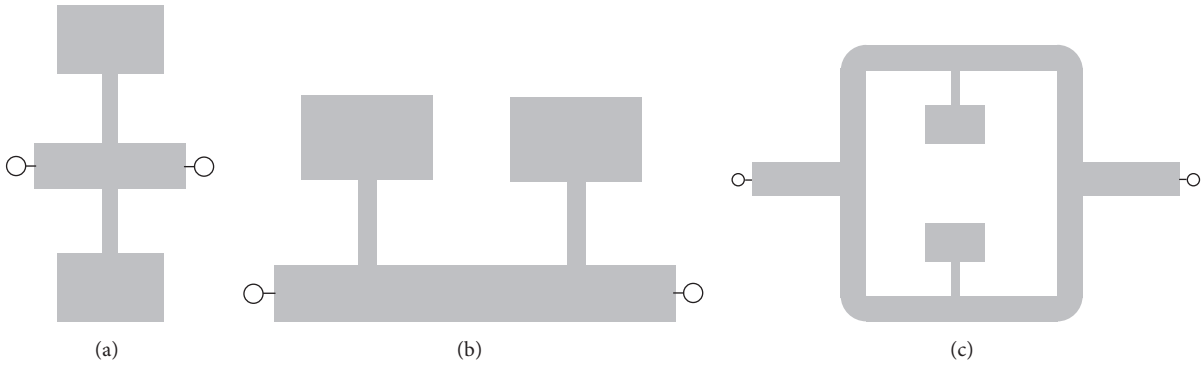

Figure 2: Various topologies of sensors based on microstrip lines loaded with SIRs. (a) Parallel configuration; (b) cascaded configuration; (c) splitter/combiner configuration.

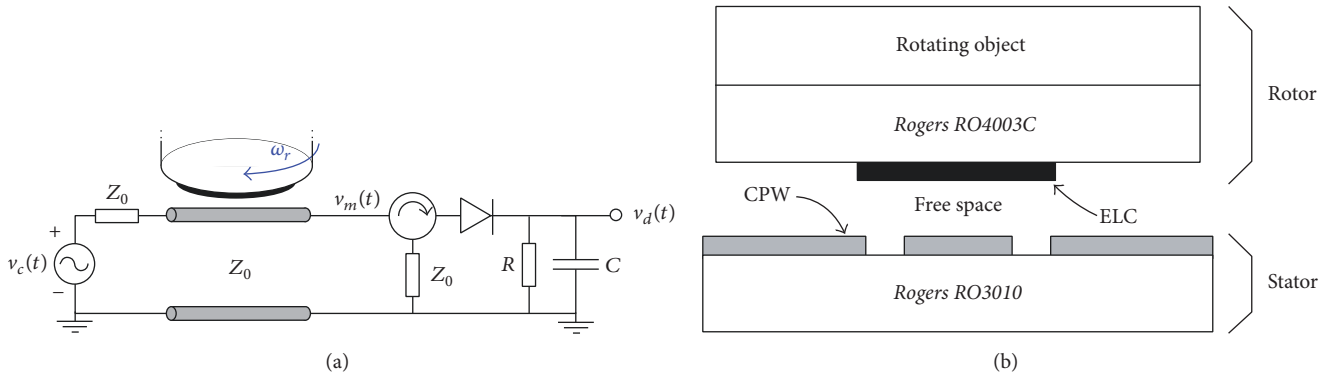

Figure 3: Schematic for the angular velocity measurement (axial configuration) (a) and cross section of the active part of the sensor (b).

to it. The amplitude of the feeding signal at the output port of the line depends on the level of coupling between the line and the resonant element. Namely, if the coupling is negligible, the line is transparent, and the amplitude at the output port is maximized. Conversely, if the coupling is significant, the injected signal is reflected back to the source, minimizing the amplitude of the output signal. Thus, line-to-resonator coupling effectively modulates the amplitude of the output signal, and this can be used for sensing purposes. Specifically, these amplitude modulation sensors are very appropriate for measuring angular velocities [31, 32, 37, 38]. One possible approach consists of using a symmetric resonant element exhibiting an electric wall at the fundamental resonance frequency, attached to a rotating object (rotor) in an axial configuration [32, 37, 38]. By placing the rotor in close proximity to the stator, a transmission line with a magnetic wall at its symmetry plane (e.g., a CPW transmission line), the coupling between the line and the resonator depends on the relative orientation between the symmetry planes of the line and resonator and hence on the angular position of the rotor. Since each time the axial plane of the line and the symmetry plane of the resonator are aligned the amplitude of the output signal is a maximum, and this occurs twice per cycle, it follows that the angular velocity can be inferred from the envelope of the modulated signal. To this end, a circulator and an envelope detector, implemented by means of a diode,

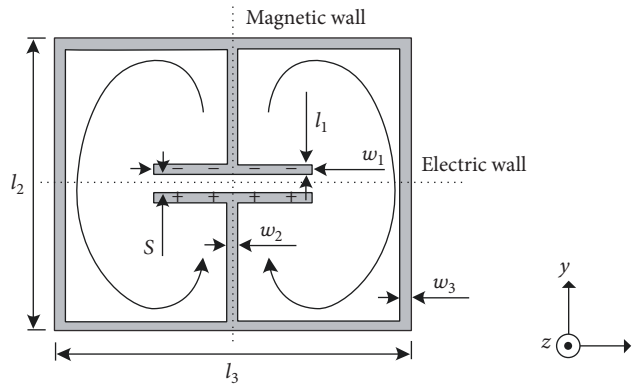

Figure 4: Topology of the bisymmetric ELC resonator with indication of charges and current flow at the fundamental resonance frequency.

are used. The circulator is sandwiched between the line and the detector, in order to prevent reflected signals from the diode. The schematic of the structure is depicted in Figure 3.

An appropriate resonator for the implementation of these angular velocity sensors is the so-called electric LC (ELC) resonator [19]. This resonant particle (see Figure 4) is bisymmetric, exhibiting an electric wall and a magnetic wall at the fundamental resonance. According to Section 2.2,

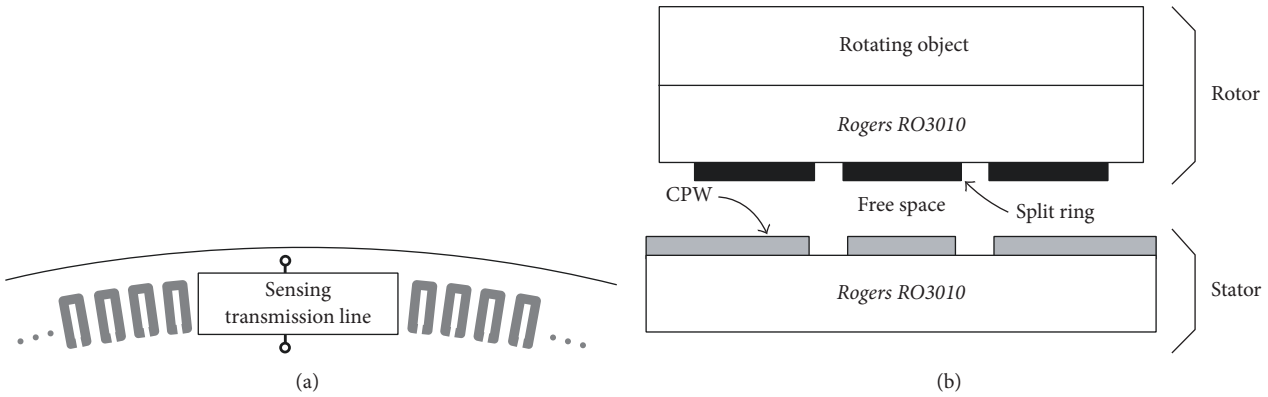

Figure 5: Perimetric configuration. (a) Top view scheme; (b) cross-sectional view.

when the electric wall of the ELC is aligned with the axial plane of the line, coupling is prevented and the line is transparent. Contrarily, the coupling is a maximum, and the transmission is a minimum, for an ELC angle corresponding to perfect alignment between the axial plane of the line and the magnetic wall of the resonant element. If both the ELC and the line are circularly shaped, the linearity between the amplitude of the output signal (in logarithmic scale) and the rotation angle is quite linear, and the sensor can be used for the measurement of angular position as well.

Alternatively to the axial configuration, the amplitude modulation based angular velocity sensors can be implemented by considering a chain of resonant elements distributed along the perimeter of the rotating object (rotor) [31]. In this case, the resonant elements must be oriented such that the coupling between the line (stator) and the resonator is maximized when the resonator is perfectly aligned with the axial plane of the line. Each time such alignment occurs, the amplitude (envelope) of the output signal is minimum, and hence the angular velocity can be inferred from the time between adjacent minimums (or maximums) and the number of resonant elements distributed along the circular chain. By this means, it is possible to measure instantaneous angular velocities with good accuracy, provided a large number of resonant elements in the rotor are considered. The schematic of the perimetric configuration is identical to the one shown in Figure 3, with the exception of the position of the stator (transmission line), which in this case is positioned in the external perimeter of the rotor, as indicated in Figure 5.

3. Examples of Applications

In this section, some examples of applications of the previous sensing strategies are given.

3.1. Examples of Sensors Based on Frequency Variation. The variation of the resonance frequency in SRR- and CSRR-loaded lines has been considered for sensing purposes. These resonators exhibit high sensitivity and are therefore good candidates for the implementation of sensors. By loading a microstrip line with a triangularly shaped CSRR, the coupling capacitance between the line and the resonator strongly depends on the relative position between the line and the CSRR. Hence, these resonators can be used as displacement sensors. The idea, pointed out in [28], where a two-dimensional displacement sensor was proposed, consists of etching the triangular CSRRs on a movable substrate, different from the one where the line is etched. By this means, a relative motion between the line and the CSRRs can be achieved. In order to achieve sensing in two dimensions, a bended microstrip line was considered in [28], and two CSRRs in the separated substrate were etched as well. One of the CSRRs is in close proximity to one of the line sections, whereas the other one is in close proximity to the other line section, as depicted in Figure 6.

Note that two orthogonally polarized receiving and transmitting antennas were cascaded to the input and output ports of the host line in order to provide a wireless connection between the sensor and the source. Figure 6(c) shows the variation of the frequency response that is obtained by laterally displacing one of the rings with regard to the line axis.

Another example concerns sensors able to spatially resolve the dielectric properties of a material. It has been achieved in [29] by loading a line with an array of SRRs tuned at different frequencies. In such sensors, a frequency shift of one individual resonant peak indicates the dielectric properties of the material under test and its location within the array. One of the structures considered in [29] is depicted in Figure 7 and corresponds to a transmission line loaded with two SRRs. In the figure, the presence of pig lung tissue can be observed in the sensitive region of one of the SRRs. Figure 7(b) shows the response of a similar structure with four SRRs and pig lung tissue in one of them. The variation of the corresponding resonance peak can be appreciated, indicating the presence of a different material on top of the sensitive region of the SRR.

Finally, CSRR-loaded microstrip lines can be used as sensors to characterize dielectric samples [39–42], particularly microwave substrates (used for circuit implementation). In these sensors, the dielectric constant is determined from the shift of the resonance frequency experienced when the material under test is placed in contact with the CSRR of the line. Such dielectric constant can be inferred through

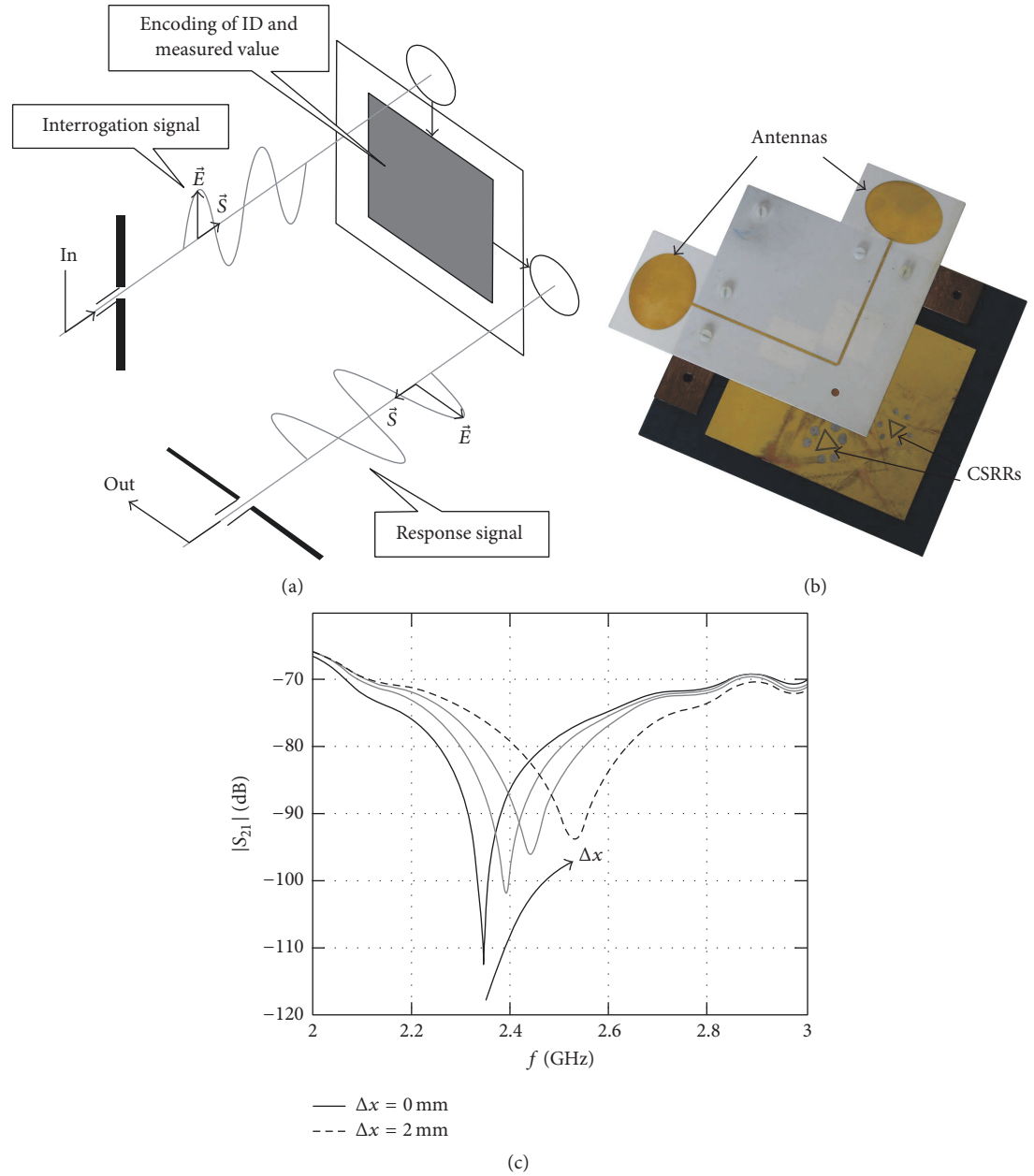

FIGURE 6: Two-dimensional wireless displacement sensor based on detuning of triangularly shaped CSRRs. (a) Scheme showing the polarization decoupling of interrogation and response signals; (b) photograph; (c) frequency response for various displacement values. For better visualization in (b), the movable sensitive plate was rotated 180°. Reprinted with permission from [28].

a calibration curve, by considering dielectric slabs with known permittivity. However, if the dielectric constant of the substrate is known, it is possible to obtain the dielectric constant of the sample under test (SUT) from the following expression:

$$\varepsilon_{\text{SUT}} = 1 + \frac{\left(\omega_0'^{-2} - \omega_0^{-2}\right)}{L_c C_c}\left(1 + \varepsilon_r\right), \tag{1}$$

where L_c and C_c are the inductance and capacitance of the CSRR in the CSRR-loaded line without SUT, ε_r is the dielectric constant of the substrate, and ω_0 and ω_0' are the notch frequencies of the structure without and with SUT, respectively. As an example, the CSRR-loaded line of Figure 8 has been loaded with a dielectric sample (SUT) corresponding to an identical substrate to that of the line (*Rogers RO3010* with dielectric constant 10.2). The measured response of the line with and without the SUT is depicted in Figure 8(b). In the structure without the SUT, L_c and C_c have been inferred from the parameter extraction method reported in [43]. Thus, expression (1) can be evaluated, and the dielectric constant of the SUT has been found to be $\varepsilon_{\text{SUT}} = 9.39$, in good agreement with the nominal value. It is worth

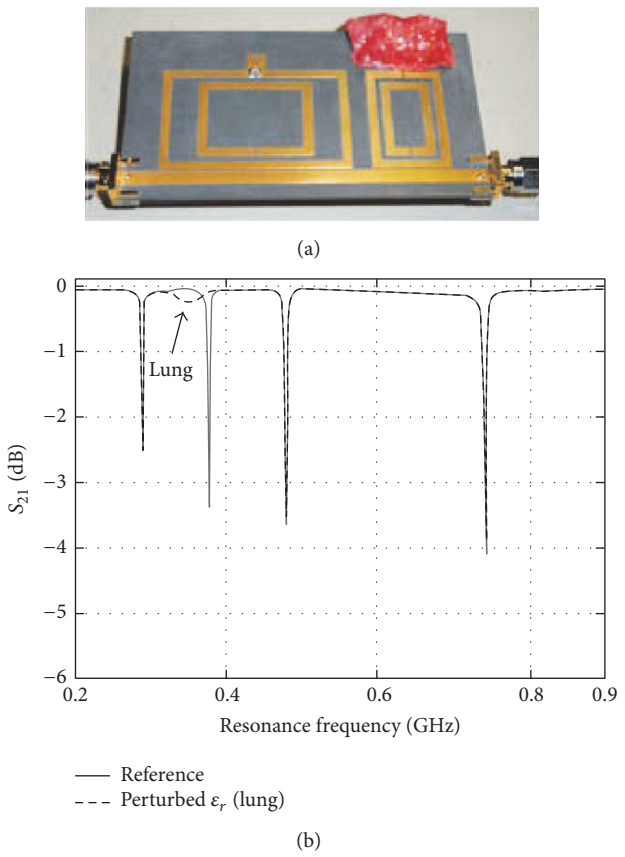

FIGURE 7: (a) Transmission line loaded with two SRRs and pig lung tissue on top of the sensitive region of one of the SRRs; (b) frequency response for the case of 4 SRRs loading the line. Reprinted with permission from [29].

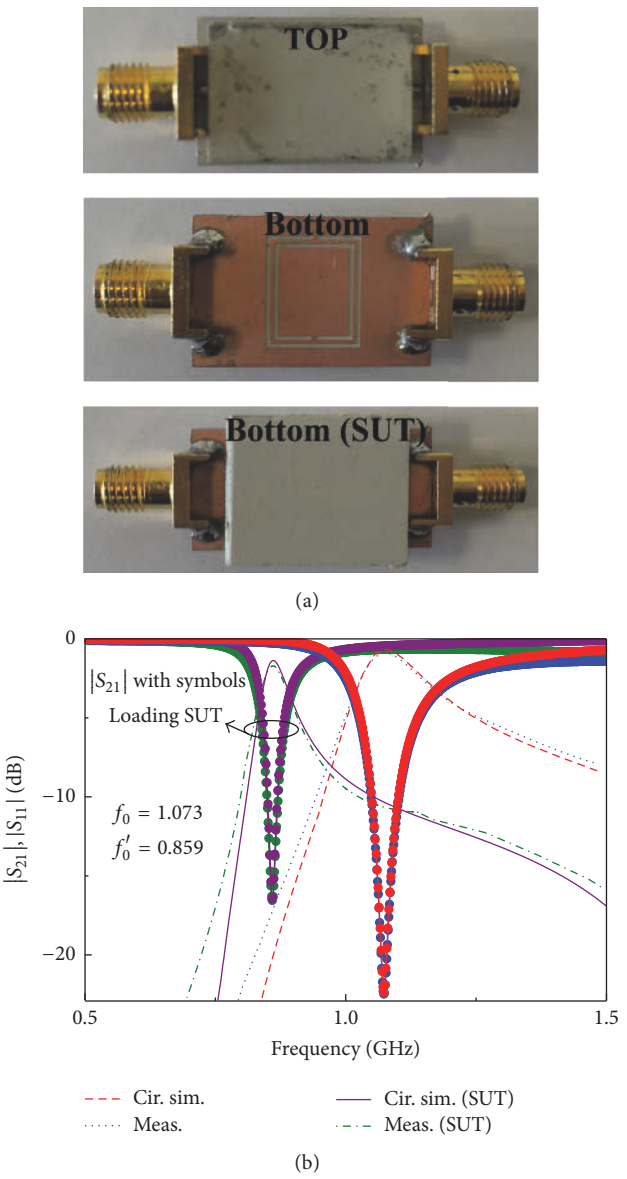

FIGURE 8: CSRR-loaded line used as permittivity sensor (a) and insertion and return loss (b). The reactive elements values are C_c = 6.81 pF and L_c = 2.42 nH. Note that in the top view the metallic strip of the microstrip line is not visible since it is covered by a piece of slab with the same parameters as the substrate. This has been done in order to have a homogeneous material surrounding the line strip, resulting in an embedded microstrip line, required in this application.

mentioning that we have repeated the measurements several times by putting pressure to the SUT in order to minimize the effects of the air gap and the results are stable.

3.2. Examples of Sensors Based on Coupling Modulation. Several types of sensors based on coupling modulation have been reported [24–27, 32]. Most of them use the transmission coefficient of a transmission line loaded with one or several resonant elements. A different approach is used in [27], where a two-dimensional displacement and alignment sensor is implemented on the basis of the reflection coefficients of orthogonally oriented open microstrip lines loaded with SRRs. The layout of the device is depicted in Figure 9. For the unperturbed state, the resonators are not excited and the injected signals to both ports are reflected back to the source. Hence, the reflection coefficients are $|S_{11}| = |S_{22}| = 1$. However, if the alignment is broken by displacement in the x- and y-directions, the SRRs will be excited and notches will appear in the reflection coefficients. Further displacement in the x- and y-directions gives rise to a stronger coupling between the transmission lines and the SRRs, in turn resulting in deeper notches in the reflection coefficients at the resonance frequency of the SRRs. These notches result from radiation effects, and this is another relevant feature of this sensing strategy based on (one-port) open-ended transmission lines.

Note that displacement in the x-direction has no effect on the depth of notch in $|S_{22}|$ (nor displacement in the y-direction onto $|S_{11}|$). Thus, misalignment in the x- and y-directions can be independently sensed from the depth of notches in $|S_{11}|$ and $|S_{22}|$, respectively. One advantage of this method is that both SRRs can be designed to operate at the same resonance frequency. This is in contrast to the previous two-dimensional displacement sensor based on the

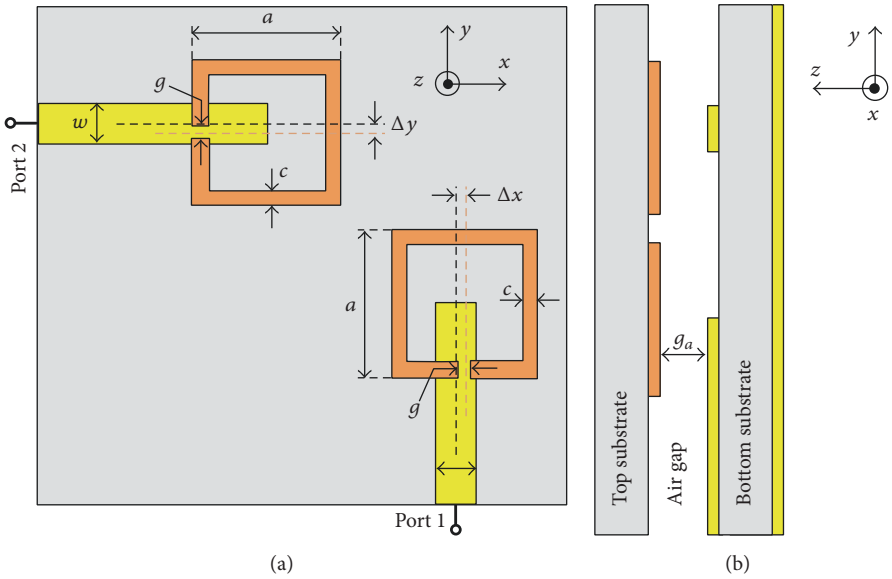

FIGURE 9: Top (a) and side (b) views of the two-dimensional displacement sensor based on the resonance in the reflection coefficients. The structures are patterned on *Rogers RO4003* substrates with 0.81 mm thickness. The geometrical dimensions of the line and SRR are w = 1.84 mm, a = 7 mm, g = 0.5 mm, and c = 0.5 mm. There is an air gap with g_a = 0.76 mm between the two substrates. Reprinted with permission from [27].

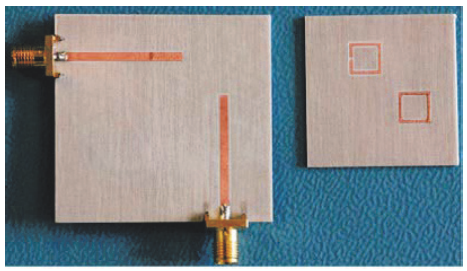

FIGURE 10: Photograph of the fabricated sensor implemented through open-ended transmission lines. Reprinted with permission from [27].

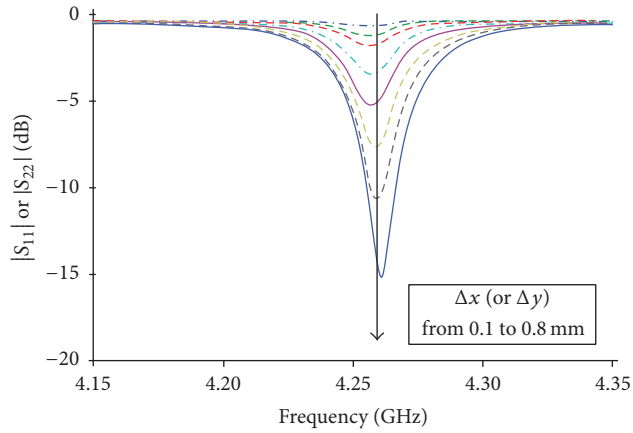

FIGURE 11: Measured $|S_{11}|$ (or $|S_{22}|$) for different values of displacement Δx (or Δy) from 0.1 to 0.8 mm in steps of 0.1 mm. Reprinted with permission from [27].

transmission characteristics of a CPW, where SRRs needed to have distinct resonance frequencies. Note that the direction of motion cannot be determined with the sensor depicted in Figure 9. Nevertheless, additional resonant elements, tuned at different frequencies, can be added to the movable substrate in order to distinguish the directions of motion.

The photograph of the fabricated device is shown in Figure 10. Figure 11 depicts the reflection coefficient measured from any of the ports for different lateral displacement values (seen from the corresponding port). One important feature of the proposed sensor is that displacement affects only the depth of the notch and leaves the resonance frequency nearly intact. A fixed resonance frequency is an important feature that enables the proposed sensor to operate at a fixed frequency. This invariability of the resonance frequency is due to the fact that such frequency mainly depends on the characteristics of the SRRs, rather than on their coupling to the line. However, for some resonators and lines, the SRRs may be affected by the presence of the line and this invariability is not always guaranteed.

3.3. Examples of Sensors Based on Frequency Splitting. Let us consider in this section frequency splitting sensors based on splitter/combiner structures loaded with SIRs [30]. The same type of sensors implemented by loading the splitter/combiners with CSRRs is reported in [36]. The photograph and frequency response of one of these sensors without loading on top of the SIRs are depicted in Figure 12. It can be appreciated that a single notch in the frequency response appears, as expected on account of symmetry. However, when symmetry is disrupted, the single notch is split into two

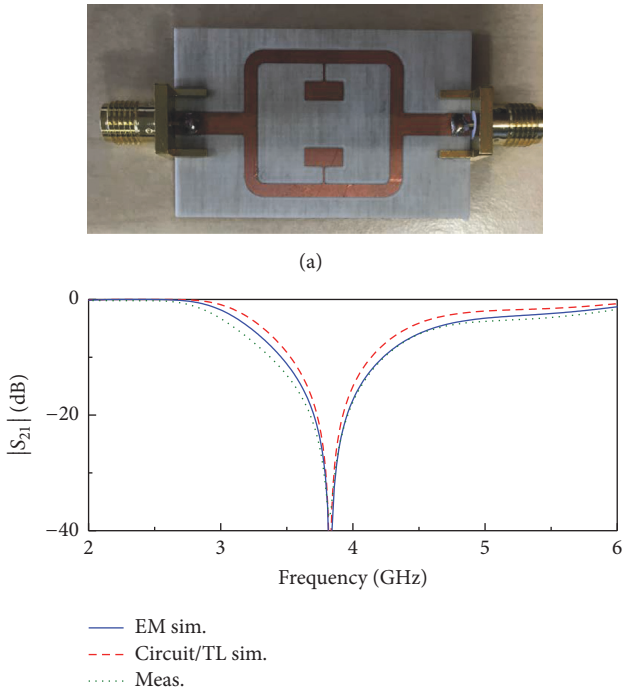

FIGURE 12: Fabricated splitter/combiner based sensor (a) and insertion loss (b). The structure has been fabricated on the *Rogers RO4003C* substrate with thickness $h = 812.8\ \mu$m and dielectric constant $\varepsilon_r = 3.38$. Reprinted with permission from [30].

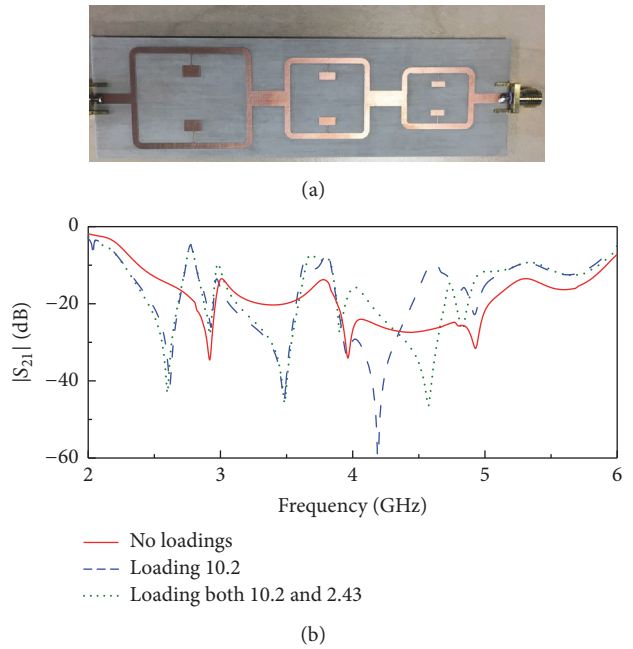

FIGURE 13: Fabricated trisection splitter/combiner sensor (a) and measured response (insertion loss), compared with the response that results by loading one of the SIRs of each pair with a dielectric slab of dielectric constant 10.2 and by loading both SIRs of each pair with dielectric slabs of different dielectric constants (10.2 and 2.43) (b). Reprinted with permission from [30].

notches. This is illustrated in Figure 13, where a trisection splitter/combiner structure is depicted, and the response to different loading combinations is reported. To this end, a dielectric slab (a square-shaped piece of unmetalized *Rogers RO3010* substrate with thickness $h = 1.27$ mm and dielectric constant $\varepsilon_r = 10.2$) has been added on top of one of the SIRs of each pair. With these unbalanced loads, frequency splitting of the three resonance frequencies of the SIRs is expected, and this is confirmed from the measured response, also included in Figure 13. Then, each pair of SIRs has been loaded with unbalanced loads, but in this case considering dielectric slabs with different dielectric constants (i.e., square-shaped pieces of unmetalized *Rogers RO3010* substrate with thickness $h = 1.27$ mm and dielectric constant $\varepsilon_r = 10.2$ and *Arlon CuClad 250 LX* with $\varepsilon_r = 2.43$ and $h = 0.49$ mm). Again, frequency splitting (see Figure 13) points out the difference in the dielectric constants of both slabs loading the different pairs of SIRs. To summarize, note that in the red curve only three notches are present, indicating that no loading is present in the three pairs of resonant elements. However, for the other curves, three pairs of notches appear as a consequence of unbalanced loads in the three pairs of resonant elements.

3.4. Examples of Sensors Based on Amplitude Modulation. In this section, an amplitude modulation based sensor potentially useful for the measurement of the angular velocity in reaction wheels of spatial vehicles is presented [31]. For that application, the perimetric configuration is more convenient than the axial configuration for two main reasons: (i) from a mechanical viewpoint, the axial configuration is more complex since the axial region of the wheels may contain the rotating axis, or other mechanical elements for rotation; (ii) with the perimetric configuration, the measurement of instantaneous velocities is possible, and the accuracy is determined by the number of resonant elements of the perimetric chain (see Section 2.4).

The sensor is based on a broadside coupled SRR (BC-SRR) loaded coplanar waveguide (CPW) (Figure 14(a)). The stator is a CPW loaded with a pair of split rings, whereas the rotor consists of a periodic circular chain of split rings, identical to those of the stator but rotated 180°. The cross-sectional view scheme of the assembly is indicated in Figure 14(b). Note that this configuration is not exactly the one indicated in Figure 5(b). The justification is as follows: in order to measure quasi-instantaneous angular velocities, the space between adjacent rings must be minimized. If a CPW is coupled directly to an array of split rings, as indicated in Figure 5(b), there are two cross-coupling effects: (i) the CPW is simultaneously coupled to multiple resonators and (ii) neighboring resonators are coupled to each other. Using the reported approach, both parasitic effects can be ignored; namely, the CPW is coupled only to the BC-SRRs and the interresonator coupling is at frequencies higher than the frequency of interest, f_0, the resonance frequency of the BC-SRR, which must be the frequency of the harmonic signal injected to the CPW. Figure 14(c) shows the insertion loss of the CPW at f_0 for different relative displacement values

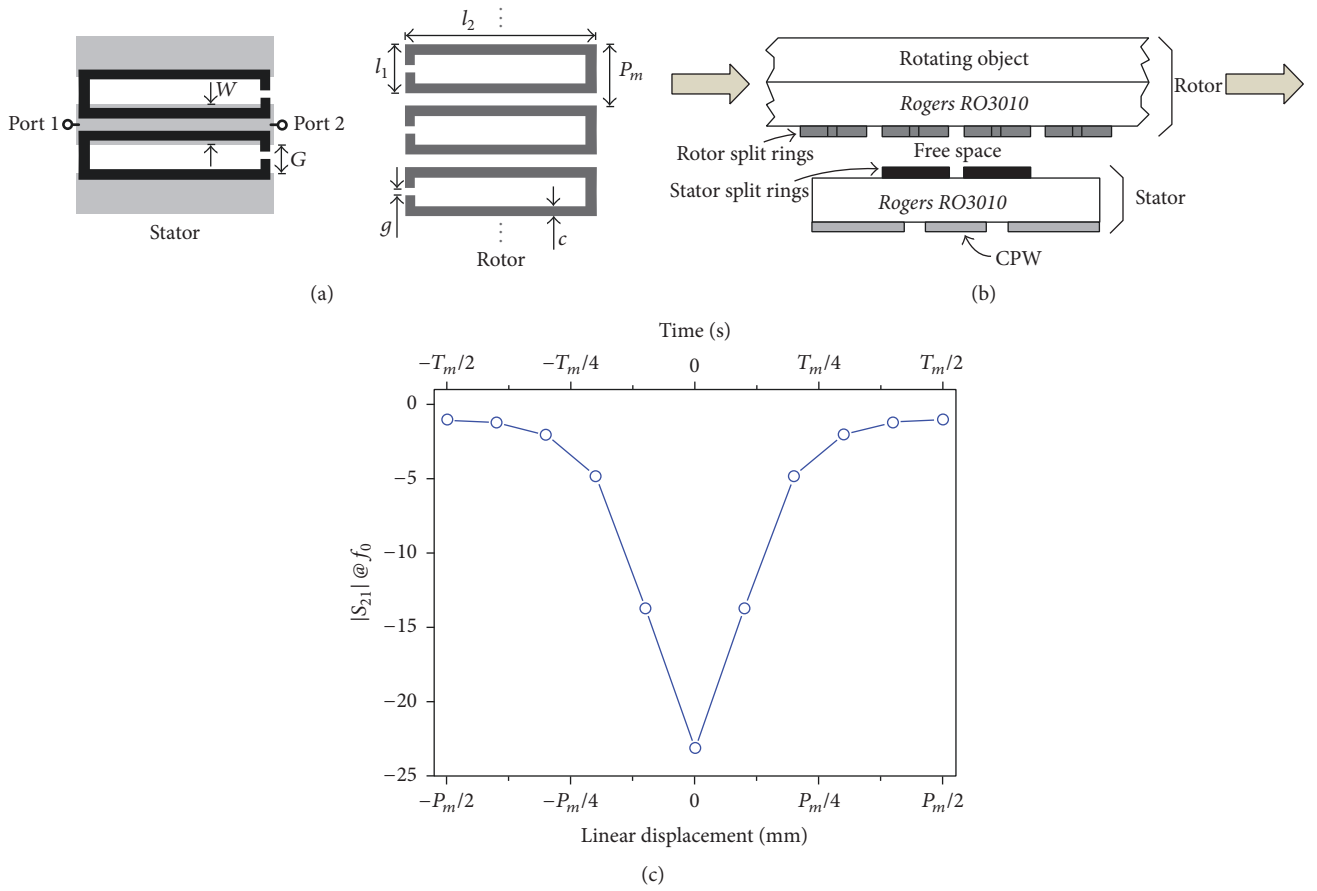

FIGURE 14: Layout of the stator and rotor parts (a), scheme of the cross-sectional view, indicating the direction of motion of the rotor (b), and insertion loss at f_0 for different displacement values (0 mm displacement corresponds to the reference position). Reprinted with permission from [31].

between the rings of the rotor and those of the stator. It can be appreciated that maximum attenuation occurs for the reference position, defined as that in which a pair of rotor rings are aligned with the pair of stator rings, forming a perfect (aligned) BC-SRR.

The prototype of the sensor can be seen in Figure 15, where a chain of 300 resonators is etched over a 101.6 mm radius rotor. The experimental setup consists of a signal generator (*Agilent* E4438C), a Schottky diode (*Avago HSMS-2860*), an oscilloscope (*Agilent MSO-X-3104A*), and a stepper motor (*STM 23Q-3AN*) to control the displacement and velocity of the rotor. Figure 16 depicts the measured envelope function for a 3,000 rpm angular speed, where it can be appreciated that the period corresponds to this velocity, taking into account the number of resonators of the chain.

4. Discussion

Let us briefly discuss some advantages of the sensors considered in the previous section. The use of metamaterial-inspired resonators for the implementation of sensors based on frequency variation has the main advantage of resonator size. This is especially critical in applications such as the one reported in Figure 7 (sensors to spatially resolve the dielectric properties of a material). Moreover, these resonant elements (SRRs, CSRRs, etc.) typically exhibit good sensitivity (i.e., variation of frequency with dielectric properties or with spatial variables). Particularly, the use of CSRR for measuring dielectric properties of slabs, or even liquids [36, 39–41, 44], is very convenient since the capacitance (and hence resonance frequency) of these resonant elements is very sensitive to the presence of a dielectric load on top of the resonators.

In sensors based on coupling modulation or frequency splitting, the main advantage is that these sensors are similar to differential-mode sensors, and therefore they are robust in front of cross-sensitivities caused by external factors, since variations in variables related to ambient factors such as temperature or moisture have effects that are seen as common mode stimulus. Both sensor types are very useful as comparators as well. It is worth mentioning that coupling modulation sensors are more sensitive to noise, as compared to frequency splitting sensors, since the output variable is the notch depth. Nevertheless, the typical sensitivities and dynamic ranges of these coupling modulation sensors applied to the measurement of spatial variables have been found to be reasonable. Frequency splitting sensors are less sensitive

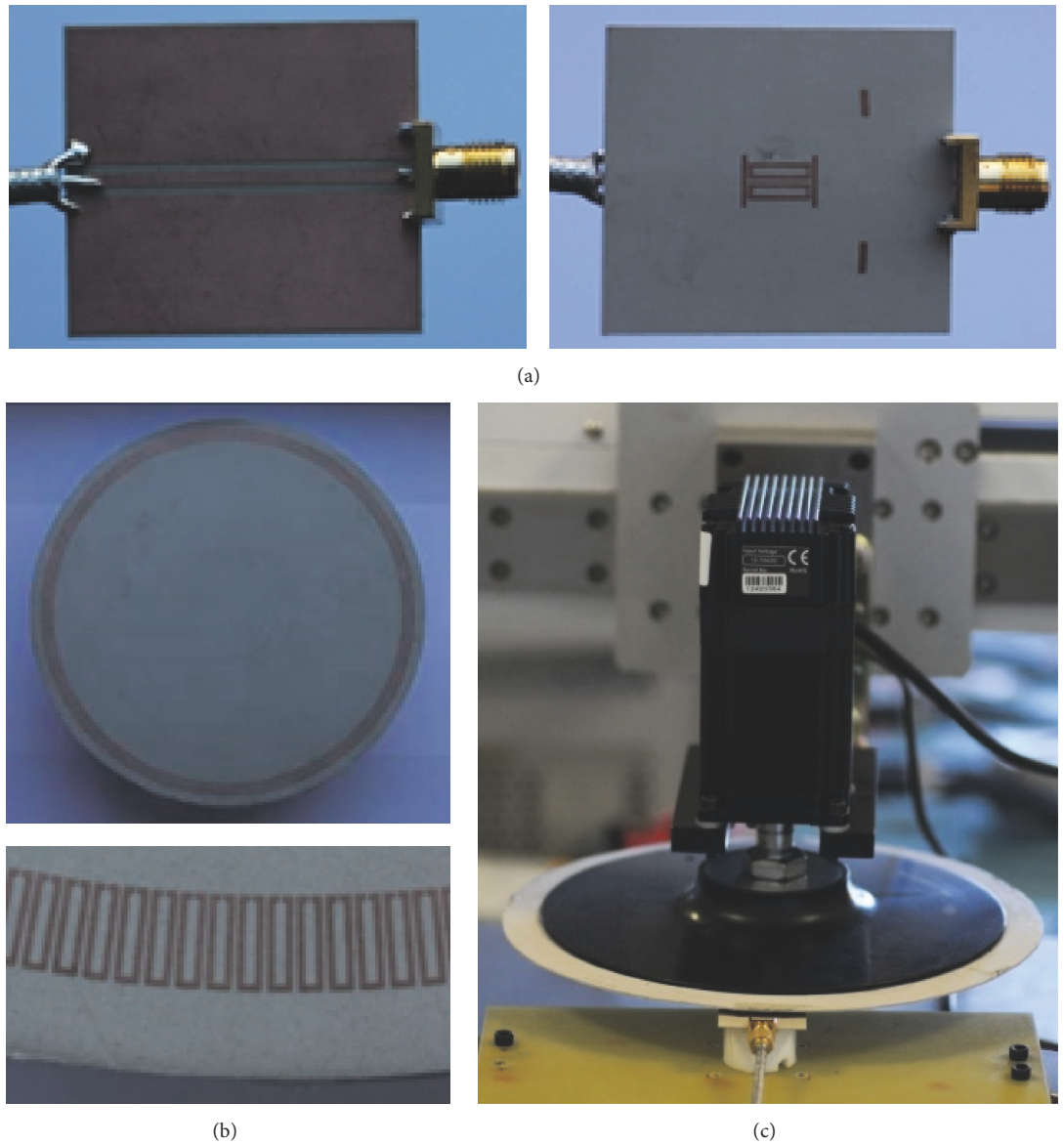

(a)

(b)

(c)

Figure 15: (a) Stator, (b) rotor, and (c) assembly of the prototype. Via holes and strips connecting the CPW ground planes are used to suppress the slot mode. Calibration marks on the stator are visible.

to noise and are suitable for real-time differential measurements. Moreover, it has been demonstrated that these sensors can be used for measuring several samples simultaneously.

Finally, the latter sensors of the previous section, based on amplitude modulation, can be considered a particular case of coupling modulation sensors, where the output variable is contained in the envelope function of an amplitude modulated carrier signal. The particular application is the measurement of the angular velocity, based on the distance between pulses in the envelope function. One figure of merit of these sensors is the number of pulses, which provides the angle resolution and determines the capability of the sensor to detect fast changes in the instantaneous angular velocity. In the proposed sensor, 300 pulses are considered, but this number can be enhanced by adding further resonant elements in an additional SRR chain (concentric but displaced one semiperiod as compared to the one of Figure 15(b)) and an additional SRR pair in the rotor. As compared to optical encoders, these sensors are cheaper. As compared to angular velocity sensors based on potentiometers, the proposed sensors do not suffer from mechanical friction and hence are more robust against aging effects.

5. Conclusions

In conclusion, several sensing strategies for the implementation of microwave sensors based on metamaterial-inspired resonators have been reviewed, and examples of applications have been provided. Particularly, the reviewed sensors are useful for material characterization and as displacement and velocity sensors. Of interest for telecommunication circuits and space applications are the frequency variation sensors

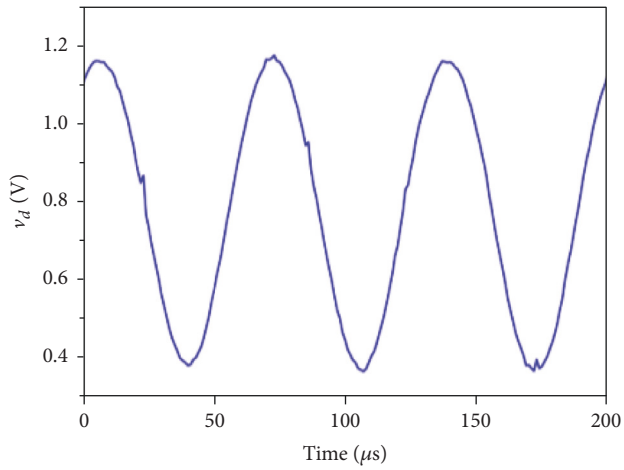

Figure 16: Measured envelope function for a 3,000 rpm speed. Reprinted with permission from [31].

based on CSRRs, useful to determine the dielectric constant of microwave substrates, and the amplitude modulation sensors based on BC-SRRs, which are able to provide the angular velocity of rotating cylinders and are therefore of potential interest to replace optical sensors in reaction wheels, or for the determination of the angular position in pointing mechanisms, among others.

Conflicts of Interest

The authors declare that they have no conflicts of interest regarding the publication of this paper.

Acknowledgments

This work has been supported by MINECO-Spain (Projects TEC2013-40600-R and TEC2016-75650-R) and by Generalitat de Catalunya (Project 2014SGR-157). Ferran Martín has been awarded with an ICREA Academia Award. The work has been also supported by FEDER funds. Lijuan Su acknowledges the China Scholarship Council (CSC) for Grant 201306950011.

References

[1] R. Marqués, F. Martín, and M. Sorolla, *Metamaterials with Negative Parameters: Theory, Design, and Microwave Applications*, John Wiley, 2007.

[2] M. Aznabet, M. Navarro-Cía, S. A. Kuznetsov et al., "Polypropylene-substrate-based SRR- And CSRR-metasurfaces for submillimeter waves," *Optics Express*, vol. 16, no. 22, pp. 18312–18319, 2008.

[3] J. D. Baena, L. Jelinek, R. Marqués, and J. Zehentner, "Electrically small isotropic three-dimensional magnetic resonators for metamaterial design," *Applied Physics Letters*, vol. 88, Article ID 134108, 2006.

[4] R. A. Shelby, D. R. Smith, and S. Schultz, "Experimental verification of a negative index of refraction," *Science*, vol. 292, no. 5514, pp. 77–79, 2001.

[5] F. Martín, F. Falcone, J. Bonache, R. Marqués, and M. Sorolla, "Split ring resonator-based left-handed coplanar waveguide," *Applied Physics Letters*, vol. 83, no. 22, pp. 4652–4654, 2003.

[6] G. Zamora, S. Zuffanelli, F. Paredes, F. J. Herraiz-Martinez, F. Martin, and J. Bonache, "Fundamental-mode leaky-wave antenna (LWA) using slotline and split-ring-resonator (SRR)-based metamaterials," *IEEE Antennas and Wireless Propagation Letters*, vol. 12, pp. 1424–1427, 2013.

[7] D. R. Smith, W. J. Padilla, D. C. Vier, S. C. Nemat-Nasser, and S. Schultz, "Composite medium with simultaneously negative permeability and permittivity," *Physical Review Letters*, vol. 84, no. 18, pp. 4184–4187, 2000.

[8] D. Schurig, J. J. Mock, B. J. Justice et al., "Metamaterial electromagnetic cloak at microwave frequencies," *Science*, vol. 314, no. 5801, pp. 977–980, 2006.

[9] M. Gil, C. Damm, A. Giere et al., "Electrically tunable split-ring resonators at microwave frequencies based on barium-strontium-titanate thick films," *Electronics Letters*, vol. 45, no. 8, pp. 417-418, 2009.

[10] M. Gil, C. Damm, M. Sazegar et al., "Tunable sub-wavelength resonators based on barium-strontium-titanate thick-film technology," *IET Microwaves, Antennas and Propagation*, vol. 5, no. 3, pp. 316–323, 2011.

[11] C. Damm, M. Maasch, R. Gonzalo, and R. Jakoby, "Tunable composite right/left-handed leaky wave antenna based on a rectangular waveguide using liquid crystals," in *Proceedings of the IEEE MTT-S International Microwave Symposium, (MTT '10)*, pp. 13–16, usa, May 2010.

[12] M. Roig, M. Maasch, C. Damm, O. H. Karabey, and R. Jakoby, "Liquid crystal based tunable composite right/left-handed leaky-wave antenna for Ka-Band applications," in *Proceedings of the 43rd European Microwave Conference (EuMC '13)*, pp. 759–762, Nuremberg, Germany, October 2013.

[13] R. Alaee, M. Farhat, C. Rockstuhl, and F. Lederer, "A perfect absorber made of a graphene micro-ribbon metamaterial," *Optics Express*, vol. 20, no. 27, pp. 28017–28024, 2012.

[14] D. Bouyge, D. Mardivirin, J. Bonache et al., "Split ring resonators (SRRs) based on micro-electro-mechanical deflectable cantilever-type rings: application to tunable stopband filters," *IEEE Microwave and Wireless Components Letters*, vol. 21, no. 5, pp. 243–245, 2011.

[15] D. Bouyge, A. Crunteanu, M. Durán-Sindreu et al., "Reconfigurable split rings based on MEMS switches and their application to tunable filters," *Journal of Optics (United Kingdom)*, vol. 14, no. 11, Article ID 114001, 2012.

[16] J. B. Pendry, A. J. Holden, D. J. Robbins, and W. J. Stewart, "Magnetism from conductors and enhanced nonlinear phenomena," *IEEE Transactions on Microwave Theory and Techniques*, vol. 47, no. 11, pp. 2075–2084, 1999.

[17] F. Falcone, T. Lopetegi, J. D. Baena, R. Marqués, F. Martín, and M. Sorolla, "Effective negative-ε stopband microstrip lines based on complementary split ring resonators," *IEEE Microwave and Wireless Components Letters*, vol. 14, no. 6, pp. 280–282, 2004.

[18] R. Marqués, F. Medina, and R. Rafii-El-Idrissi, "Role of bianisotropy in negative permeability and left-handed metamaterials," *Physical Review B*, vol. 65, Article ID 144440, 2002.

[19] D. Schurig, J. J. Mock, and D. R. Smith, "Electric-field-coupled resonators for negative permittivity metamaterials," *Applied Physics Letters*, vol. 88, no. 4, Article ID 041109, 2006.

[20] H. Chen, L. Ran, J. Huangfu et al., "Left-handed materials composed of only S-shaped resonators," *Physical Review E*, vol. 70, Article ID 057605, 2004.

[21] M. Makimoto and S. Yamashita, "Compact bandpass filters using stepped impedance resonators," *Proceedings of the IEEE*, vol. 67, no. 1, pp. 16–19, 1977.

[22] F. Martín, *Artificial Transmission Lines for RF and Microwave Applications*, John Wiley, Hoboken, NJ, USA, 2015.

[23] J. Naqui, *Symmetry Properties in Transmission Lines Loaded with Electrically Small Resonators: Circuit Modeling and Applications*, Springer Theses, 2016.

[24] J. Naqui, M. Durán-Sindreu, and F. Martín, "Novel sensors based on the symmetry properties of split ring resonators (SRRs)," *Sensors*, vol. 11, no. 8, pp. 7545–7553, 2011.

[25] J. Naqui, M. Durán-Sindreu, and F. Martín, "Alignment and position sensors based on split ring resonators," *Sensors*, vol. 12, no. 9, pp. 11790–11797, 2012.

[26] A. Karami-Horestani, C. Fumeaux, S. F. Al-Sarawi, and D. Abbott, "Displacement sensor based on diamond-shaped tapered split ring resonator," *IEEE Sensors Journal*, vol. 13, no. 4, pp. 1153–1160, 2013.

[27] A. K. Horestani, J. Naqui, D. Abbott, C. Fumeaux, and F. Martín, "Two-dimensional displacement and alignment sensor based on reflection coefficients of open microstrip lines loaded with split ring resonators," *IET Electronics Letters*, vol. 50, no. 8, pp. 620–622, 2014.

[28] C. Mandel, B. Kubina, M. Schüßler, and R. Jakoby, "Passive chipless wireless sensor for two-dimensional displacement measurement," in *Proceedings of the 41st European Microwave Conference*, pp. 79–82, Manchester, UK, 2011.

[29] M. Puentes, C. Weiss, M. Schussler, and R. Jakoby, "Sensor array based on split ring resonators for analysis of organic tissues," in *proceddings of the IEEE/MTT-S International Microwave Symposium (MTT '11)*, Baltimore, Md, USA, June 2011.

[30] L. Su, J. Mata-Contreras, P. Vélez, and F. Martín, "Configurations of splitter/combiner microstrip sections loaded with stepped impedance resonators (sirs) for sensing applications," *Sensors*, vol. 16, no. 12, article 2195 pages, 2016.

[31] J. Naqui and F. Martín, "Application of broadside-coupled split ring resonator (BC-SRR) loaded transmission lines to the design of rotary encoders for space applications," in *Proeedings of the IEEE/MTT-S International Microwave Symposium (IMS' 11)*, San Francisco, Calif, USA, May 2016.

[32] J. Naqui and F. Martín, "Transmission lines loaded with bisymmetric resonators and their application to angular displacement and velocity sensors," *IEEE Transactions on Microwave Theory and Techniques*, vol. 61, no. 12, pp. 4700–4713, 2013.

[33] G. Urban, *Handbook of Modern Sensors: Physics, Designs, and Applications*, Springer, New York, NY, USA, 3rd edition, 2004.

[34] J. Naqui, C. Damm, A. Wiens, R. Jakoby, L. Su, and F. Martin, "Transmission lines loaded with pairs of magnetically coupled stepped impedance resonators (SIRs): modeling and application to microwave sensors," in *Proceedings of the 2014 IEEE MTT-S International Microwave Symposium (IMS '14)*, Tampa, Fla, USA, June 2014.

[35] J. Naqui, C. Damm, A. Wiens et al., "Transmission lines loaded with pairs of stepped impedance resonators: modeling and application to differential permittivity measurements," *IEEE Transactions on Microwave Theory and Techniques*, vol. 64, no. 11, pp. 3864–3877, 2016.

[36] L. Su, J. Naqui, J. Mata-Contreras, and F. Martin, "Splitter/combiner microstrip sections loaded with pairs of complementary split ring resonators (CSRRs): modeling and optimization for differential sensing applications," *IEEE Transactions on Microwave Theory and Techniques*, vol. 64, no. 12, pp. 4362–4370, December 2016.

[37] J. Naqui and F. Martín, "Angular displacement and velocity sensors based on electric-LC (ELC) loaded microstrip lines," *IEEE Sensors Journal*, vol. 14, no. 4, pp. 939-940, 2014.

[38] J. Naqui, J. Coromina, A. Karami-Horestani, C. Fumeaux, and F. Martín, "Angular displacement and velocity sensors based on coplanar waveguides (CPWs) loaded with S-shaped split ring resonators (S-SRR)," *Sensors*, vol. 15, no. 5, pp. 9628–9650, 2015.

[39] M. S. Boybay and O. M. Ramahi, "Material characterization using complementary split-ring resonators," *IEEE Transactions on Instrumentation and Measurement*, vol. 61, no. 11, pp. 3039–3046, 2012.

[40] C.-S. Lee and C.-L. Yang, "Complementary split-ring resonators for measuring dielectric constants and loss tangents," *IEEE Microwave and Wireless Components Letters*, vol. 24, no. 8, pp. 563–565, 2014.

[41] A. Ebrahimi, W. Withayachumnankul, S. Al-Sarawi, and D. Abbott, "High-sensitivity metamaterial-inspired sensor for microfluidic dielectric characterization," *IEEE Sensors Journal*, vol. 14, no. 5, pp. 1345–1351, 2014.

[42] C.-L. Yang, C.-S. Lee, K.-W. Chen, and K.-Z. Chen, "Noncontact measurement of complex permittivity and thickness by using planar resonators," *IEEE Transactions on Microwave Theory and Techniques*, vol. 64, no. 1, pp. 247–257, 2016.

[43] J. Bonache, M. Gil, I. Gil, J. Garcia-Garcia, and F. Martin, "On the electrical characteristics of complementary metamaterial resonators," *IEEE Microwave and Wireless Components Letters*, vol. 16, no. 10, pp. 543–545, 2006.

[44] A. Salim and S. Lim, "Complementary Split-Ring Resonator-Loaded Microfluidic Ethanol Chemical Sensor," *Sensors*, vol. 16, no. 12, pp. 1–13, 2016.